Materials Science and Engineering C 32 (2012) 1222–1229

Contents lists available at SciVerse ScienceDirect

Materials Science and Engineering C

journal homepage: www.elsevier.com/locate/msec

Cobalt-based orthopaedic alloys: Relationship between forming route, microstructure and tribological performance

Bhairav Patel [a], Gregory Favaro [b], Fawad Inam [c,d,1], Michael J. Reece [d], Arash Angadji [e], William Bonfield [f], Jie Huang [a], Mohan Edirisinghe [a,*]

[a] Department of Mechanical Engineering, University College London, Torrington Place, London WC1E 7JE, UK
[b] CSM Instruments SA, Rue de la Gare 4, Galileo Center, CH-2034 Peseux, Switzerland
[c] Advanced Composite Training and Development Centre and School of Mechanical and Aeronautical Engineering, Glyndŵr University, Mold Road, Wrexham LL11 2AW, UK
[d] School of Engineering and Materials Science and Nanoforce Technology Ltd, Queen Mary University of London, London E1 4NS, UK
[e] Orthopaedic Research UK, Furlong House, 10a Chandos Street, London W1G 9DQ, UK
[f] Department of Materials Science and Metallurgy, University of Cambridge, Pembroke Street, Cambridge CB2 3QZ, UK

ARTICLE INFO

Article history:
Received 24 January 2012
Received in revised form 10 March 2012
Accepted 18 March 2012
Available online 27 March 2012

Keywords:
Metallic
Orthopaedic
Forming
Microstructure
Tribology
Spark plasma sintering

ABSTRACT

The average longevity of hip replacement devices is approximately 10–15 years, which generally depends on many factors. But for younger generation patients this would mean that revisions may be required at some stage in order to maintain functional activity. Therefore, research is required to increase the longevity to around 25–30 years; a target that was initially set by John Charnley. The main issues related to metal-on-metal (MoM) hip replacement devices are the high wear rates when malpositioned and the release of metallic ions into the blood stream and surrounding tissues. Work is required to reduce the wear rates and limit the amount of metallic ions being leached out of the current MoM materials, to be able to produce an ideal hip replacement material. The most commonly used MoM material is the cobalt-based alloys, more specifically ASTM F75, due to their excellent wear and corrosion resistance. They are either fabricated using the cast or wrought method, however powder processing of these alloys has been shown to improve the properties. One powder processing technique used is spark plasma sintering, which utilises electric current Joule heating to produce high heating rates to sinter powders to form an alloy. Two conventionally manufactured alloys (ASTM F75 and ASTM F1537) and a spark plasma sintered (SPS) alloy were evaluated for their microstructure, hardness, tribological performance and the release of metallic content. The SPS alloy with oxides and not carbides in its microstructure had the higher hardness, which resulted in the lowest wear and friction coefficient, with lower amounts of chromium and molybdenum detected from the wear debris compared to the ASTM F75 and ASTM F1537. In addition the wear debris size and size distribution of the SPS alloy generated were considerably small, indicating a material that exhibits excellent performance and more favourable compared to the current conventional cobalt based alloys used in orthopaedics.

1. Introduction

The performance of metal-on-metal (MoM) hip replacement devices reported over the last decade has shown excellent results in terms of longevity of the implants, with most devices lasting around 15 years [1]. For the older generation, this may seem sufficient, but with an increase in the number of younger patients being fitted with hip replacement devices, the longevity of these implants needs to be increased to almost double the existing longevity [2]. One of the most fundamental problems with these devices is the higher wear rates compared to a ceramic-on-ceramic (CoC) bearing combination [3]. The most common method of failure of these devices is through aseptic loosening of the implant. This is caused due to the wear debris of the material. Therefore, wear is one of the most important factors to be considered. It has been shown that limiting the wear factor can play an important role in the long term viability of the implant [4]. Another factor that has caused major problems for the metallic materials for hip replacement devices is the release of metallic ions [5]. Even though it has been suggested, no proof has been shown that indicates metallic ions cause damage to the surrounding areas, resulting in sarcomas or necrosis [6]. However, the release of ions may not be ideal in terms of excess amounts of ionic content circulating the human system. All metallic materials release metallic ions over time, and limiting these ions would significantly improve the biocompatibility and reduce the risk of failure of the implant and enable patients to be satisfied with the new device in the long

* Corresponding author. Tel.: +44 20 76793942; fax: +44 20 73880180.
E-mail address: m.edirisinghe@ucl.ac.uk (M. Edirisinghe).
[1] When work was carried out author was at affiliation d.

0928-4931/$ – see front matter © 2012 Elsevier B.V. All rights reserved.
doi:10.1016/j.msec.2012.03.012

term. Passivity layers on the surface of the material that protect against degradation become broken due to the wearing process and the metallic ions are released due to metal–blood interactions [7]. Therefore, research is required into limiting the wear rate and release of metallic ions of MoM hip replacement devices and to increase the life span of these implants.

The most common MoM hip replacement device materials are the cobalt based alloys, and more specifically the cobalt–chromium–molybdenum (Co–Cr–Mo) system [5]. The most commercially used alloy for clinical application is the cast version of Co28Cr6Mo (ASTM F75) and the wrought versions ASTM F1537 and ASTM F799 [8–12]. These alloys have been used extensively and have shown to be a good choice of material for bearing surfaces, due to their excellent mechanical, corrosion and especially wear resistance properties [13,14]. Metallic alloy properties are determined by their microstructure, which can be enhanced by coating the surface, heat treatment, deforming the alloy, or controlling the processing conditions [15–18]. Controlling the processing conditions has shown to significantly improve the mechanical properties of the alloy [19]. There are various methods of processing alloys: casting, forging, powder processing. Casting is a simple process of heating the material above its melting point and pouring the molten liquid into a set die and allowing it to cool. This process does not have much scope for variability to produce different microstructures resulting in improved properties. Wrought production is the forging or working of the cast ingot either hot or cold. This has been known to improve the properties, by plastically deforming the material and increasing the strengths of the material [20]. Powder processing is the one method that provides the user the ability to control many factors to produce significantly improved properties [21].

One powder processing technique that has the ability to significantly improve the properties via microstructural control is spark plasma sintering (SPS). This sintering technique utilises electric current to provide energy to the powders to enable sintering to occur [22]. A pulsed DC current is applied through a conductive graphite die and sintering is initiated via the Joule effect, through high intensity energy [23]. The energy is transformed into heat energy that drives the sintering process and enables even distribution of heat throughout, external through the graphite die and internal through the powders. Various materials have been processed for structural and functional uses and many innovative materials have been fabricated using this process [24]. This process can sinter materials at fast heating and cooling rates and with high pressures, which can limit grain growth resulting in production of samples with improved performance [25]. It is also a very cost effective method as processing time is reduced significantly compared to conventional sintering [26]. It can also produce highly dense materials at low temperatures and be able to produce favourable phases [27,28]. Patel et al. have shown that producing the F75 composition of the cobalt based alloy via SPS has yielded a microstructure that has hardness closer to that of ceramic materials used in hip replacement devices [29]. In this work, the tribological properties of the powder processed alloy are tested against the commercially used cobalt based alloy to determine its performance in terms of wear and the release of metallic content.

2. Experimental details

2.1. Materials

Three alloys were used in this work: ASTM F75 (Weartech, UK), ASTM F1537 (Lamineries Matthey SA, Switzerland) and an alloy produced via spark plasma sintering (referred in this article as the SPS alloy). This alloy was sintered at 1075 °C, with a dwell time of 10 min and a pressure of 100 MPa. This condition was chosen, as it is the optimum condition based upon work conducted by Patel et al. [29]. The counter piece used for the wear test is alumina (Atlas Ball and Bearing, UK). The elemental content of the commercial grade alloys stated by the suppliers is shown in Table 1. The three metallic materials were formed into a 20 mm × 3 mm disc and the alumina was in the form of a 6 mm diameter ball. Three samples of each material were used for testing.

2.2. Microstructure characterisation and phase analysis

The three alloys were evaluated for their microstructure and phase analysis. The microstructure was analysed using scanning electron microscopy (Hitachi S-3400N (SEM)). The phase analysis was conducted with an X'PERT PRO Philips diffractometer operating with CuKα radiation at 45 kV and 40 mA in the scanning range of 30–90° with a step size of 0.03° and a scan time of 400 s per data point.

2.3. Microhardness and nanohardness

Microhardness was measured using a Leco M-400-G instrument with the Vickers indentation method (ASTM E92) [30]. Five measurements were taken on all the alloys. Nanohardness was measured using a CSM Instruments Nano Hardness Tester (CSM Instruments, Switzerland) with a diamond Berkovich indenter with a linear loading/unloading rate of 100 mN/min and maximum load of 50 mN. The nanohardness was calculated through the load/displacement curves and the Oliver and Pharr method [31]. Five measurements were taken on all the alloys.

2.4. Wear test

Wear testing was conducted using a CSM Instruments Tribometer (CSM Instruments, Switzerland). The discs were polished using silicon carbide paper from 120 to 4000P grade. The initial surface roughness was analysed using a ConScan surface profilometer. The average roughness (R_a) was measured at 0.015 μm, 0.01 μm and 0.01 μm for the F75, F1537 and SPS alloys, which is lower than the 0.05 μm maximum recommended (ASTM Standard F732) [32].

Three samples of each alloy were tested against the 6 mm diameter Al_2O_3 ball under the ASTM G133 and ASTM F732 standards [32,33]. The wear mode was a rotational motion with a 1.5 mm radius, linear speed of 0.04 m/s and a normal load of 5 N. Temperature was set at 37 °C with a humidity of 40%. The sliding distance was ~2.4 km (250,000 laps). Both alloys and balls were cleaned with isopropanol before wear testing commenced. The lubricating fluid was 25 wt.% bovine serum (Sigma Aldrich, UK) with distilled water and 0.01 wt.% sodium azide (Sigma Aldrich, UK). Serum was collected after testing and frozen for wear particle analysis. The wear rate was measured using the equation $V_i = k_i\ F\ s$ [34]: where V_i is the wear volume, F is the normal load, s is the sliding distance and k_i is the specific wear rate coefficient. The total wear volume was measured using the wear profile. The wear profile was constructed using a ConScan surface profilometer (CSM Instruments, Switzerland). Images of the wear track were taken using SEM (Hitachi S-3400N).

Table 1
Elemental content (wt.%) of ASTM F75 and ASTM F1537 alloys as indicated by the suppliers. In the case of the SPS alloy the attempted composition mimics the ASTM F75 composition but is C free.

Alloy	Cobalt (Co)	Chromium (Cr)	Molybdenum (Mo)	Carbon (C)	Other elements
F75	Balance	30%	6%	0.20%	0.80%
F1537	Balance	27%	6%	0.04%	1.8%

2.5. Wear particle analysis

The wear particles were analysed for their size and size distribution using Nanosight LM10-HS (Nanosight, UK). 1 ml of unfrozen serum was diluted ×100,000 using Pure Water (Rathburn Chemicals Ltd, Walkerburn). Serum analysis for metal element concentration was conducted using a high-resolution ICP-MS instrument (Element2; Thermo Finnigan, Bremen, Germany). Acid oxidative digestion was used to digest the material within the serum for analysis, including the metallic nanoparticles, the proteins and other insoluble materials. 0.5 ml of extracted serum fluid was digested with 5 ml of nitric acid (Super Purity Solvents grade, Romil) at 100 °C for 240 min, using a dry heating block (DigiPrep, SCP Science, Quebec, Canada). After digestion, the remaining fluid was further diluted to 20 ml, ready for analysis. The concentrations of the metal elements are expressed in μg/l.

3. Results and discussion

3.1. Microstructure and phase analysis

The three alloys: F75, F1537 and SPS alloys were evaluated for their microstructure and phases. The F75 and F1537 alloys are the commercially used alloys in hip replacement devices. The F75 alloy is manufactured by the traditional casting method [35]. The F1537 alloy is manufactured using the wrought method, either hot or warm, and can be annealed or unannealed [10]. Their microstructures (Fig. 1a, b) show similarities due to the similar elemental content (Table 1). The microstructures consist of a solid cobalt matrix with interdendritic phases and carbides. The carbides are a combination of either cobalt (Co), chromium (Cr) or molybdenum (Mo) and carbon and are denoted as M_nC_n where M is either Co, Cr or Mo.

The F1537 comes in two types, either low carbon (LC) or high carbon (HC), depending upon the C content. LC is typically <0.05% and HC is typically >0.2% [10]. The increased C content increases the strengths of the alloy by reducing dislocation movement; therefore the HC alloy has increased wear resistance [36,37]. The F1537 alloy used in this study is of the LC type as indicated in Table 1, with the C content <0.05%. X-ray diffraction (XRD) of the F75 and F1537 (Fig. 2) shows the same phases, they consist of the face centred cubic (FCC) Co, $M_{23}C_6$ and sigma (σ). The other alloy is the SPS alloy, manufactured by Patel et al. using nanopowders and spark plasma sintering [29]. The microstructure of the SPS alloy (Fig. 1c) prepared differs from that produced by conventional sintering. Analysis from the XRD phases (Fig. 2), gives an indication of the phases present in the microstructure. The phases are FCC Co, hexagonal closed packed (HCP) Co, Cr, Mo and chromium oxide (Cr_2O_3).

Some of the phases formed in the F75, F1537 and SPS alloys coincide with those predicted by the phase diagram of the Co–Cr–Mo system [38,39]. The phase diagrams for this cobalt system (Co28Cr6Mo) show that at low temperatures (~650 °C) the most likely phases to form are the HCP Co and σ phases. As the temperature increases (~950 °C) further the phases likely to form are σ, HCP Co and FCC Co (γ) phases. With further increase of temperature (1200 °C), the γ Co phase is most likely to form and even more increase to 1300 °C the same γ phase is the most likely to form [40,41]. In terms of the F75 and F1537, these are the phases that are mostly found in the microstructure, however, the addition of C makes carbides favour the formation of FCC Co phases (γ) rather than the more thermodynamically-predictable HCP Co phase formed at the lower temperature ends, therefore more γ phases are usually found in these alloys [42,43]. In terms of SPS, as no carbides are present the most likely phases to form are the γ, HCP Co and σ phases or a combination of these. However, only some of these phases form, such as HCP Co and γ. The Cr and Mo rich phases form as the solubility of the Cr and Mo seems to be low in the SPS alloy, whereas in the Co–Cr and Co–Mo phase diagram under the SPS sintered conditions the Cr and Mo are highly soluble and form γ phase [44]. With C present these phases are made less soluble as the C binds to form the carbides

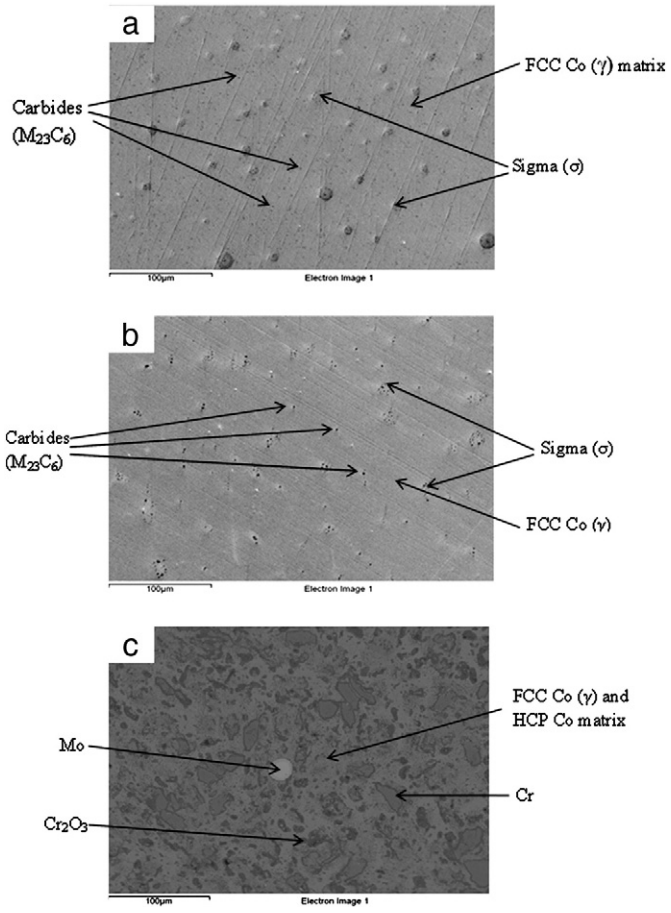

Fig. 1. Microstructure of the alloys before wear testing: (a) F75, (b) F1537 and (c) SPS alloys. Phases indicated: face centred cubic (FCC) cobalt (Co), gamma (γ), sigma (σ), carbides ($M_{23}C_6$ where M = cobalt, chromium, molybdenum and C = carbon), hexagonal close packed (HCP), cobalt (Co), chromium (Cr), molybdenum (Mo) and chromium oxide (Cr_2O_3).

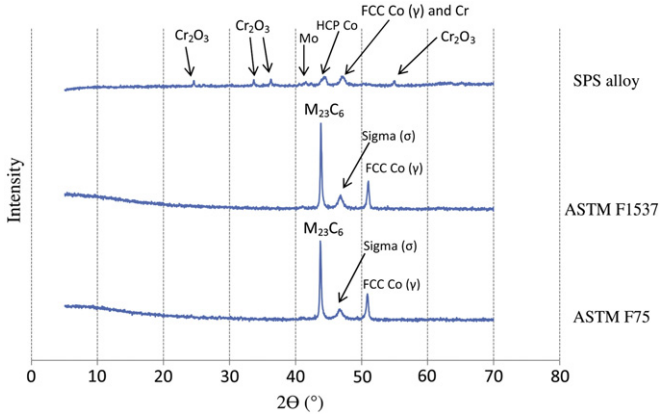

Fig. 2. X-ray diffraction (XRD) patterns of the three alloys used in the study indicating the phase present. Phases indicated: face centred cubic (FCC) cobalt (Co), gamma (γ), sigma (σ), carbides ($M_{23}C_6$ where M = cobalt, chromium, molybdenum and C = carbon), hexagonal close packed (HCP), cobalt (Co), chromium (Cr), molybdenum (Mo), and chromium oxide (Cr_2O_3).

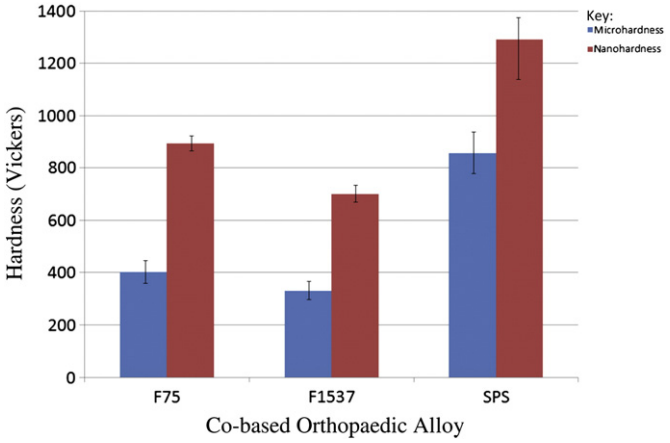

Fig. 3. Microhardness and nanohardness of F75, F1537 and SPS alloys with their error bars (standard deviation).

[45]. Another suggestion for the appearance of the Cr-rich and Mo phases is due to the insufficient time for the solid solution to form due to the fast sintering times in the SPS method. The formation of Cr_2O_3 is described by Patel et al., and is unique to the SPS system [46]. The Co powder used to form the alloy is passivated with oxygen to enable safer handling as it is very reactive when exposed to air. The sintering technique of the SPS alloy provides the means for the formation of the Cr_2O_3 phase, as the oxygen from the Co powder is displaced by the Cr due to its higher affinity for oxygen and the formation of Cr_2O_3 within the microstructure proceeds and this is favourable according to the Ellingham diagrams [47–49].

3.2. Microhardness and nanohardness

The micro- and the nano-hardness are shown in Fig. 3 which indicates that the SPS alloy has the highest micro and nano hardness. This explains that the microstructure is very hard upon the surfaces and through the top of the surface. The nanohardness, due to the small area of resistance measured, can represent the hardness of individual phases. As indicated by the standard deviation, the ASTM F75 and F1537 have small standard deviations indicating that the microstructure is uniform in terms of its hardness. The standard deviation of the SPS alloy is much larger due to the variations of the hardness. The phases within the microstructure have different hardness; within the F75 and F1537 the hardness is correlated to the carbide content as these phases are the hardest phases found in the microstructure

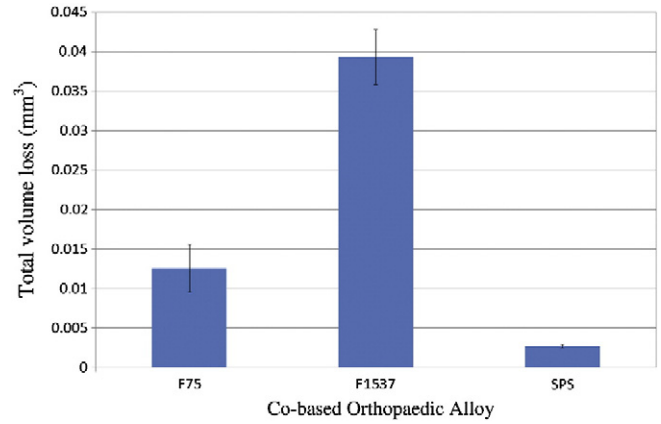

Fig. 4. Wear material loss of the F75, F1537 and SPS alloys after wear testing with their error bars (standard deviation).

Table 2
Wear rates and friction coefficient. The values in the parenthesis indicate the standard deviation.

Alloy	Wear rate ($\times 10^6$ mm^3/N m)	Mean friction coefficient (μ)
F75	1.0 (0.26)	0.18 (0.009)
F1537	2.6 (0.30)	0.21 (0.003)
SPS	0.2 (0.002)	0.17 (0.002)

[50]. For the SPS alloy the much higher hardness is attributed to the formation of the Cr_2O_3 phases [46]. This phase is a ceramic material that exhibits high corrosion resistance and high wear resistance, ideal qualities for a hip replacement device [51–53]. Compared to the carbides, this has a larger phase content and therefore can influence the hardness. The Cr_2O_3 hardness (2898 Vickers) compared to the hardness of the carbides (1200–1600 Vickers) formed in the F75

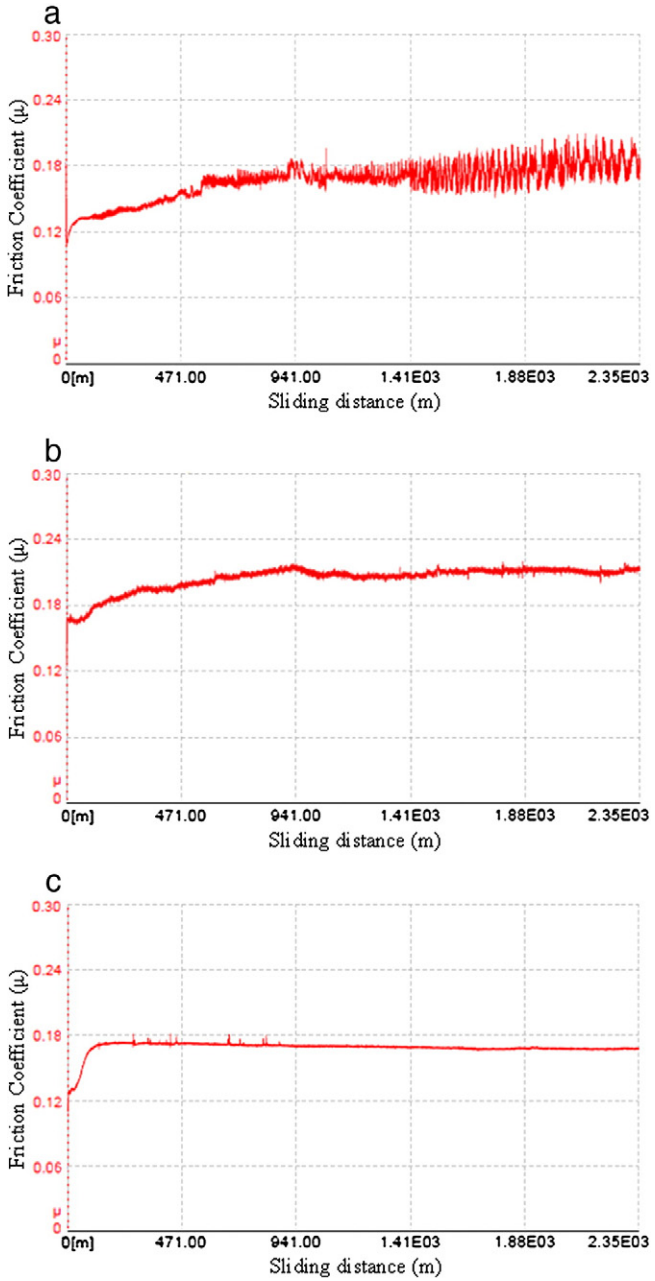

Fig. 5. Friction coefficient (μ): (a) F75, (b) F1537, and (c) SPS alloys. The friction coefficient against the sliding distance of the three alloys during wear testing.

and F1537, is much higher, therefore the oxide in the microstructure gives the alloy a higher hardness [54,55]. The Cr and Mo rich phases also help to increase the hardness as they can act as solid solution hardeners hindering dislocation movement. The HCP Co phases have fewer slip systems compared to the FCC Co, and with lower number of slip systems the dislocation movement is limited and this can increase the hardness [56,57]. The nanohardness measurements of the three alloys are higher than the microhardness measurements due to the formation of passive oxide layers. In all three alloys, due to the presence of Cr, the passive layer consists majorly of Cr_2O_3, and some minute amounts of oxides of Co and Mo [58]. This oxide as mentioned above has extreme hardness and therefore the nanoindentation measurement would have this film taken into consideration as it forms around the surface of the alloys.

3.3. Wear and friction coefficient

The total material volume loss due to wear is shown in Fig. 4. This shows that the two conventional alloys have a much higher volume loss of material compared to the SPS alloy. This can be related back to the hardness in Fig. 3. The higher hardness alloy exhibits lower loss of material, as the microstructure is more resistant to the wear. The F1537 alloy has a higher amount of wear material loss compared to the F75 alloy. The low carbon content of the F1537 alloy has been known to give a lower wear resistance compared to the higher carbon content alloys and therefore the amount of wear loss would be greater, as the main strengthening mechanism in these alloys is the carbides. This material loss can be translated into a wear rate coefficient from the equation in Section 2.4 and is shown in Table 2. This rate expresses the amount of wear material loss, over a specific distance, under a specific load. The wear rate data shows that SPS alloy has the lowest wear rate.

Table 2 also shows the friction coefficient. The low friction coefficient of the SPS alloy indicates that the contact between the surfaces has a low resistance to friction. The lower friction resistance will provide smoother contact between the surfaces and therefore reduce the wear. The friction coefficient graphs are shown in Fig. 5. The SPS alloy also has the lowest coefficient of friction which has a large influence on the wear rates as can be seen in Table 2, as they complement each other. Having a higher friction coefficient gives higher wear rates as the two surfaces in motion have increased friction and therefore present a larger resistance to movement. For smooth motion between surfaces a low friction coefficient is beneficial as it can prevent friction from occurring and provides a low energy surface [59]. It also prevents the friction to cause phase changes due to point heating as the cobalt based alloys are known to undergo phase changes after wear, transforming from a FCC phase to a HCP phase due to strain induced deformation [60,61]. The increased friction can cause the surfaces to become fused due to the heat produced during wearing and the sudden movement could remove large amounts of material. The friction coefficient graphs in Fig. 5 show how the friction coefficient changed during the wear test. In Fig. 5, all graphs have a small amount of run-in phase after which the steady state phase is formed. The F75 and F1537 (Fig. 5a, b) have more “noisy” lines, as the friction coefficient fluctuates during the test, indicating that the test runs less smoothly. The SPS alloy (Fig. 5c), has a smoother line in the steady state phase, indicating that during the test the friction coefficient remained fairly stable and the motion between the surfaces was smooth.

In hip replacement devices, one of the major failures is due to the aseptic loosening of the implant and this is related to the wear debris and high coefficient of friction [62,63]. The wear debris when still circulating near the wear region can become entrapped between the bearing surfaces and during motion this accelerates abrasive wear. The other form of wear that usually occurs is sliding wear, where no abrasive particles are involved. The images of the wear track (Fig. 6) show the type of wear that has occurred. F75 and F1537 (Fig. 6a, b) show small areas of abrasive wear, where small grooves can be seen

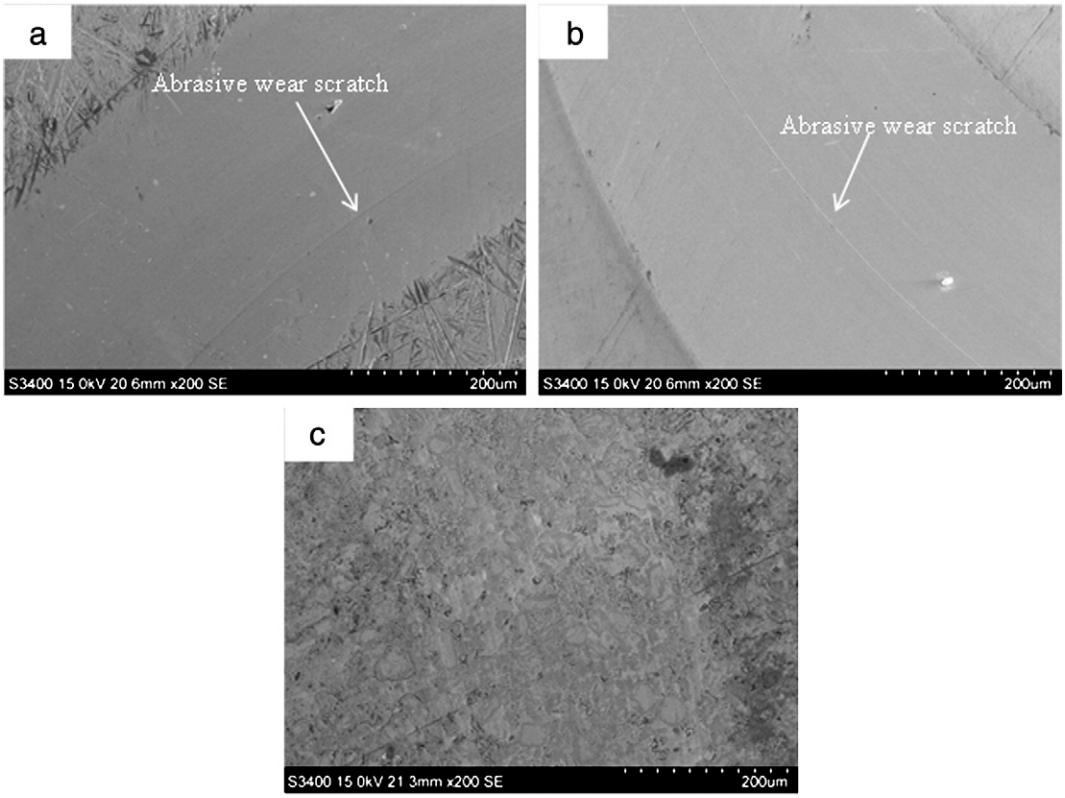

Fig. 6. SEM images of the wear tracks: (a) F75, (b) F1537, and (c) SPS alloys. SEM images of the wear track of the three alloys after wear testing, with the abrasive wear scratches indicated on the images.

identifying the marks of the particles that may have been entrapped between the surfaces, which is common in wearing of these materials, where the actebular cup or femoral head shows large striations upon the surfaces indicating large amount of abrasive wear [64,65]. The SPS alloy (Fig. 6c), has no distinctive marks of abrasive wear indicating that only sliding wear may have occurred upon the alloy. With the SPS alloy showing a lower wear rate and a coefficient of friction compared to the other conventionally manufactured alloys, the amount of wear debris produced is less and therefore the risk of aseptic loosening is reduced.

The wear profile of the three alloys is shown in Fig. 7. The cross sectional view can be used to determine how the wear has occurred. While the wear track image shows only the top surfaces with the grooves and other defects, the wear profile can indicate the amount of material loss, due to the area under the surface and the profile of the wear erosion. The F75 and F1537 wear profiles are very similar, and show a U bend shape, probably due to the hard alumina ball wearing upon the surface. The softer material enables the harder ball to penetrate deeper into the surface, and the shape of the curve can be attributed to the alumina ball. The F1537 alloy has a lower and wider depth indicating that it is a softer material compared to the F75, which can be confirmed by the hardness results (Fig. 3). The wear profile of the SPS alloy has a shallower depth and is not so rounded-off at the end, indicating that the material is being worn away more steadily, instead of being gauged out completely, representing a harder alloy.

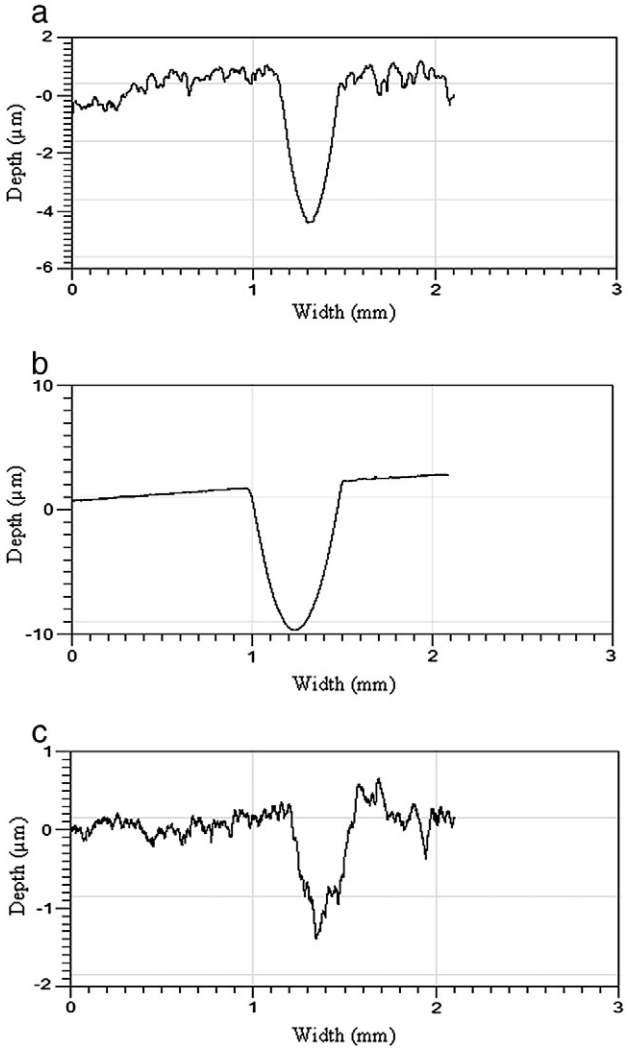

Fig. 7. Wear track profile: (a) F75, (b) F1537, and (c) SPS alloys. The cross-sectional wear track profile of the three alloys.

3.4. Wear particle analysis

The wear debris particle size of the alloys is shown in Table 3. The SPS alloy shows the smallest particle size with the smallest standard deviation. The SPS alloy shows the narrowest size distribution indicating that the particles are of more monodispersed size compared to the size distributions of the other alloys. These results are similar to the wear debris size and size distribution generated in metallic hip replacement devices [65].

The mode of the particle size distribution is in Fig. 8. In the bovine serum there are materials such as proteins, salts and other molecules and these have certain sizes. The Nanosight LM10-HS measures the particle size of all the materials present in the solution and therefore the sizes of these materials are also measured. Some researchers isolate the particles using reagents that could cause changes to the size of the particles [66,67]. The wear debris particle size is smaller than the other materials present and therefore the mode of the wear debris gives a good indication of the wear debris particle size without confusion with the other materials present. In Fig. 8a, the mode of particle size for F75 shows some peaks at the lower end around 32 nm and the main one at 60 nm, indicating that the particles could be of different sizes. The F1537 mode map (Fig. 8b), has two characteristic peaks at 22 nm and 54 nm, also indicating different sizes of particles. The SPS mode map (Fig. 8c), has one characteristic peak of 50 nm, showing that the particles are more of one size than a wider "distribution" of sizes.

The smaller the wear debris particle size, the higher the increase in the surface area for reactivity with biological material, this can be both a positive and a negative feature [68]. A larger wear debris size is harder to remove by the macrophages; therefore, requires giant cells to remove the material [69–71]. With smaller size particles, the macrophages would find it easier to engulf the foreign material ready for excretion. Also, larger material would need to be consumed and then transported, increasing the time for excretion and the processes involved [72]. The higher surface area from the smaller size particles increases the risk for reactions and therefore induces adverse effects with surrounding tissues [73,74].

The elemental content of the wear debris is shown in Fig. 9. F75 shows the lowest level of Co detected, with F1537 indicating the most Co present. The SPS debris shows a higher level of Co than the F75, but the levels of Cr and Mo are much lower than the other two alloys. The low Cr and Mo content in the SPS alloy wear debris can be attributed to the presence of Cr rich and Mo rich phases and the Cr_2O_3 phase, these phases have a high chemical stability within the matrix [75,76]. The Cr and Mo found in F75 and F1537 are found in the matrix or attributed to the carbides. The carbide formation reduces the degradation resistance of the alloy and causes the release of metallic ions into the body [77]. The level of Co and Cr found in the blood and urine of patients implanted with hip replacement devices has been a very serious issue for surgeons [78]. Reactions with their ions and compounds formed within the body have caused major problems to surrounding tissues and other organs, such as the kidneys and the liver [79–81]. The SPS alloy microstructure shows potential to produce low wear rates and also release less Cr

Table 3
Wear debris particle size details.

Alloy	Particle size (nm)	
	Mean	Standard deviation
F75	74	44
F1537	71	34
SPS	69	33

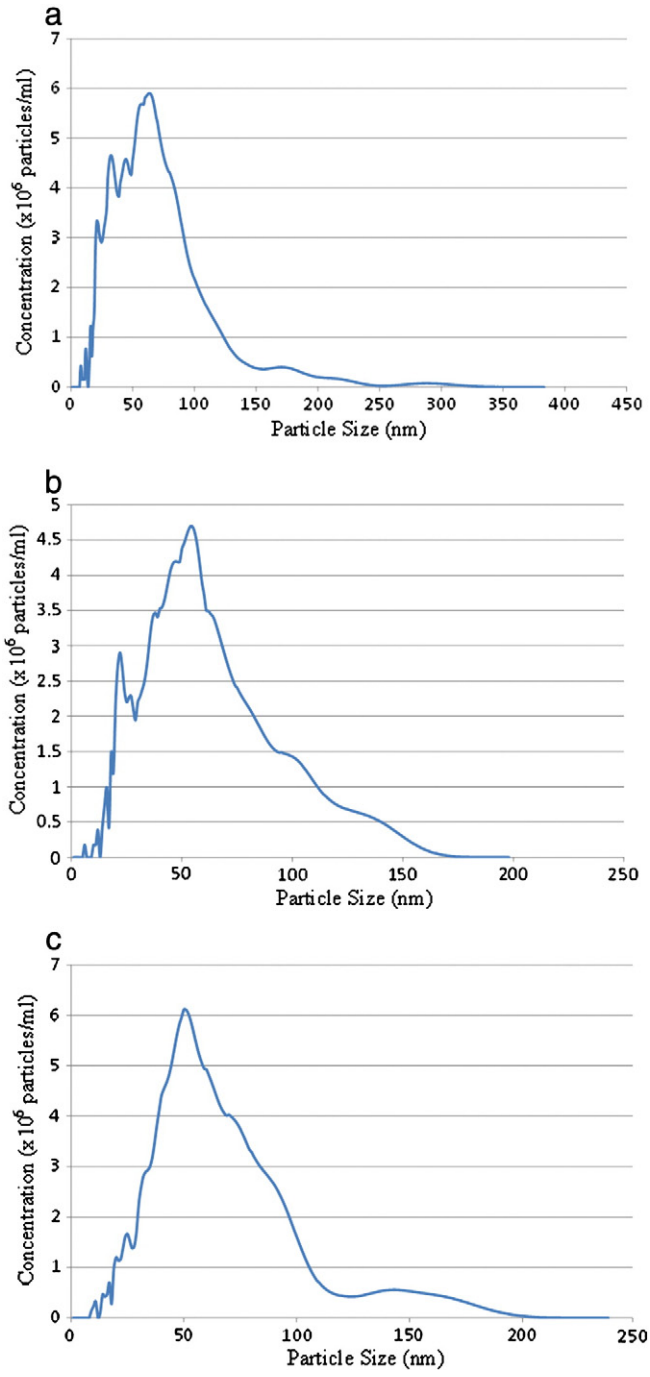

Fig. 8. Mode of wear particle debris size distribution: (a) F75, (b) F1537, and (c) SPS alloys. Concentration of the particles against the particle size is calibrated.

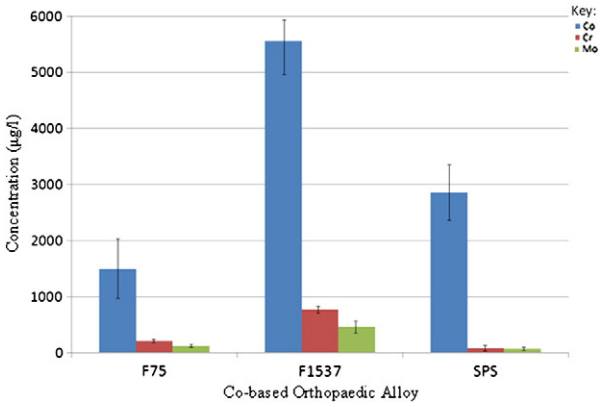

Fig. 9. Metal element content of serum after wear testing of F75, F1537 and SPS alloys. Key indicates the three elements: cobalt (Co), chromium (Cr) and molybdenum (Mo).

and Mo and therefore can have a tremendous positive impact on this problem, ensuring that the implant material for hip replacement devices is safer than the current material, causes less immune responses and therefore reducing the risk of failure and revision.

4. Conclusions

The microstructure and phase analyses of the three alloys have been studied in detail and indicate that the two conventionally manufactured alloys show similar microstructures and phases. The SPS alloy has a very different microstructure and phase content. The phases within the microstructure determine the hardness of the alloy and the similar phases of the F75 and F1537 give similar microhardness, with the F75 being slightly higher due to the increased quantity of carbon enabling more carbides to be formed. The SPS alloy was much harder, due to the specific phases, such as the HCP Co, which has few slip systems and the rich phases of Cr, Mo and Cr_2O_3 that act as dislocation movement preventers, with the oxide being the hardest phase, making the alloy even harder. The nanohardness is higher than the microhardness due to formation of passive films that these Co–Cr–Mo alloys usually form on the surface of the alloy, which consists predominantly of Cr_2O_3. The tribological performance of the three alloys has been tested and it can be observed that the SPS alloy has 5–10 times lower wear rate compared to the other two alloys. The friction coefficient of the SPS alloy is lower too giving a smoother motion between the two bearing surfaces. The wear debris particle size of the SPS alloy is smaller and has a narrower size distribution. The metallic elemental content indicates that the SPS alloy releases much less Cr and Mo compared to the F75 and F1537, but still has a relatively high Co release. Overall, the SPS alloy shows an improvement in terms of tribological performance compared to the other conventionally fabricated alloys and releases smaller amounts of the Cr and Mo. Thus, this material shows significant promise as an alternative route for production of cobalt-based (Co28Cr6Mo) orthopaedic alloys, however determining other mechanical properties such as tensile/compression strength, elongation and its fatigue resistance, which will be performed in future work, will enable a thorough resume of the alloy for orthopaedic uses.

Acknowledgements

The authors wish to thank Orthopaedic Research UK (formerly known as the Furlong Research Charitable Foundation) for funding the PhD research of Bhairav Patel. Prof. Edirisinghe also wishes to thank EPSRC (UK) for funding some parts of this work (e.g. analysis) through his platform grant (EP/E04539). Also, we would like to acknowledge Ben Owen, Nanosight Ltd. for conducting analysis in this work.

References

[1] A.A. Shinar, W.H. Harris, J. Arthroplasty 13 (1998) 243–253.
[2] J. Cawley, J.E.P. Metcalf, A.H. Jones, T.J. Band, D.S. Skupien, Wear 255 (2003) 999–1006.
[3] G.-C. Lee, A.O. Gee, J.P. Garino, US Musculoskelet. Rev. 3 (2008) 50–53.
[4] Y.T. Konttinen, D. Zhao, A. Beklen, G. Ma, M. Takagi, M. Kivelä-Rajamäki, N. Ashammakhi, Clin. Orthop. Relat. Res. 430 (2005) 28–38.
[5] D.J. Langton, S.S. Jameson, T.J. Joyce, N.J. Hallab, S. Natu, A.V.F. Nargol, Bone Joint Surg. Br. 92B (2010) 38–46.
[6] K. Merritt, A.S. Brown, Clin. Orthop. Relat. R. 329 (1996) S233–S243.

[7] T. Hanawa, Mater. Sci. Eng., C 24 (2004) 745–752.
[8] A. Marti, Injury 31 (2000) D18–D21.
[9] ASTM F75, Standard Specification for Cast Cobalt–Chromium–Molybdenum Alloy for Surgical Implant Applications, ASTM International, West Conshohocken, PA, 1998.
[10] ASTM F1537, Standard Specification for Wrought Cobalt–28Chromium–6Molybdenum Alloys for Surgical Implants, ASTM International, West Conshohocken, PA, 2000.
[11] ASTM F799, Standard Specification for Cobalt–28Chromium–6Molybdenum Alloy Forgings for Surgical Implants, ASTM International, West Conshohocken, PA, 1999.
[12] P. Huang, A. Salinas-Rodriguez, H.F. Lopez, Mater. Sci. Technol. 15 (1999) 1324–1330.
[13] A. Unsworth, in: D. Dowson, V. Wright (Eds.), An Introduction to the Biomechanics of Joints and Joint Replacement, Mechanical Engineering Publications Limited, London, 1981, pp. 134–139.
[14] H.P. Sieber, C.B. Rieker, P. Köttig, J. Bone Joint Surg. Br. 81 (1999) 46–50.
[15] J. Fisher, J.L. Tipper, M.H. Stone, C. Davies, P. Hatto, J. Bolton, M. Riley, C. Hardaker, G.H. Isaac, G. Berry, J. Mater. Sci.-Mater. Med. 15 (2004) 225–235.
[16] H.S. Dobbs, J.L.M. Robertson, J. Mater. Sci. 18 (1983) 391–401.
[17] T.M. Devine, A. Wulff, J. Biomed. Mater. Res. 9 (1975) 151–167.
[18] M. Niinomi, Metall. Mater. Trans. A 33 (2002) 477–486.
[19] M.M. Dewidar, H.C. Yoon, J.K. Lim, Met. Mater. Int. 12 (2006) 193–206.
[20] M. Semlitsch, H.G. Willert, Med. Biol. Eng. Comput. 18 (1980) 511–520.
[21] R. Brown, Cobalt News 1/4 (2001) 9–14.
[22] L.-G. Yu, K.A. Khor, H. Li, P. Cheang, Biomaterials 24 (2003) 2695–2705.
[23] D. Roy, S. Kumari, R. Mitra, I. Manna, Intermetallics 15 (2007) 1595–1605.
[24] M. Omori, Mater. Sci. Eng., A 287 (2000) 183–188.
[25] U.A. Tamburini, J.E. Garay, Z.A. Munir, Scripta Mater. 54 (2006) 823–828.
[26] M. Nygren, Z. Shen, Solid State Sci. 5 (2003) 125–131.
[27] J. Hong, L. Gao, S.D.D.L. Torre, H. Miyamoto, K. Miyamoto, Mater. Lett. 43 (2000) 27–31.
[28] Y. Harada, N. Uekawa, T. Kojima, K. Kakegawa, J. Eur. Ceram. Soc. 28 (2008) 235–240.
[29] B. Patel, F. Inam, M.J. Reece, M. Edirisinghe, W. Bonfield, J. Huang, A. Angadji, J. R. Soc. Interface 7 (2010) 1641–1645.
[30] ASTM E92, Standard Test Method for Vickers Hardness of Metallic Materials, ASTM International, West Conshohocken, PA, 2003.
[31] W.C. Oliver, G.M. Pharr, J. Mater. Res. 7 (1992) 1564–1583.
[32] ASTM F732, Standard Test Method for Wear Testing of Polymeric Materials Used in Total Joint Prostheses, ASTM International, West Conshohocken, PA, 2006.
[33] ASTM G133, Standard Test Method for Linearly Reciprocating Ball-on-Flat Sliding Wear, ASTM International, West Conshohocken, PA, 2002.
[34] J.F. Archard, J. Appl. Phys. 24 (1953) 981–988.
[35] B.D. Ratner, I. Bankman, Biomedical Engineering Desk Reference, Academic Press, Oxford, 2009.
[36] A. Frenk, W. Kurz, Wear 174 (1994) 81–91.
[37] R.M. Streicher, M. Semlitsch, R. Schon, H. Weber, C. Reiker, Proc. Inst. Mech. Eng. H 210 (1996) 223–232.
[38] K. Ragan, An Electron Microscopy Study of Phases Transformations and Room Temperature Strengthening Mechanisms in a Co–Cr–Mo–C Alloy, University of Toronto, 1974.
[39] K.P. Gupta, J. Phase Equilib. Diffus. 26 (2005) 87–92.
[40] S. Rideout, W.D. Manly, E.L. Kamen, B.S. Lement, P.A. Beek, Trans. AIME 191 (1951) 872–876.
[41] J.B. Darby Jr., P.A. Beck, Trans. AIME 203 (1955) 765–766.
[42] C. Petit, A. Taleb, M.P. Pileni, J. Phys. Chem. B 103 (1999) 1805–1810.
[43] C.P. Sullivan, M.J. Donachie, F.R. Morral, Cobalt-base SuperAlloys 1970: A Critical Survey of Cobalt Base Development with Emphasis on the Relationship of Mechanical Properties to Microstructure, Centre d'Information du Cobalt, Brussels, 1970.
[44] T.B. Massalski, Binary Alloy Phase Diagrams, ASM International, Materials Park, Ohio, USA, 1990.
[45] S. Peissl, G. Mori, H. Leitner, R. Ebner, S. Eglsaer, Mater. Corros. 57 (2006) 759–765.
[46] B. Patel, F. Inam, M.J. Reece, M. Edirisinghe, W. Bonfield, J. Huang, A. Angadji, Adv. Eng. Mater. 13 (2011) 411–417.
[47] J. Zimmermann, L.C. Ciacchi, J. Phys. Chem. Lett. 1 (2010) 2343–2348.
[48] A.G. Tyurin, Prot. Met. 39 (2003) 568–574.
[49] T.B. Reed, Free Energy of Formation of Binary Compounds, MIT Press, Cambridge, 1971.
[50] M. Dourandish, D. Godlinski, A. Simchi, V. Firouzdor, Mater. Sci. Eng., A 472 (2008) 338–346.
[51] A. Cellard, V. Garnier, G. Fantozzi, G. Baret, P. Fort, Ceram. Int. 35 (2009) 913–916.
[52] T.S. Sidhu, S. Prakash, R.D. Agrawal, Scripta Mater. 55 (2006) 179–182.
[53] D.P. Whittle, J. Stringer, Philos. Trans. R. Soc. Lond. A. 295 (1980) 309–329.
[54] J.R. Davis, Cast Irons, ASM International, Ohio, 1996.
[55] E.A. Brandes, G.B. Brook, Smithells Metals Reference Book, Butterworth-Heinemann, London, 1992.
[56] D.H. Buckley, in: A.D. Sarker (Ed.), Wear of Metals, Pergamon Press, New York, 1976, pp. 93–95.
[57] B.D. Ratner, A.S. Hoffman, J.S. Frederick, E.L. Jack, Biomaterials Science: An Introduction to Materials in Medicine, Academic Press, Oxford, 2004.
[58] A. Kocijan, I. Milosev, B. Pihlar, J. Mater. Sci.-Mater. Med. 15 (2004) 643–650.
[59] M. Streicher, M. Semlitsch, R. Schon, H. Weber, C. Rieker, Proc. Inst. Mech. Eng. 210 (1996) 223–232.
[60] R. Varan, J.D. Bobyn, J.B. Medley, S. Yue, Proc. Inst. Mech. Eng. H 220 (2006) 145–159.
[61] A. Salinas-Rodriguez, J.L. Rodriguez-Galicia, J. Biomed. Mater. Res. 31 (1996) 409–419.
[62] M. Sundfeldt, L.V. Carlsson, C.B. Johansson, P. Thomsen, C. Gretzer, Acta Orthop. 77 (2006) 177–197.
[63] M.A. McGee, D.W. Howie, K. Costi, D.R. Haynes, C.I. Wildenauer, M.J. Pearcy, J.D. McLean, Wear 241 (2000) 158–165.
[64] K.R. St. John, L.D. Zardiackas, R.A. Poggie, J. Biomed. Mater. Res. B. 68 (2004) 1–14.
[65] P.F. Doorn, P.A. Campbell, J. Worrall, P.D. Benya, H.A. McKellop, J. Biomed. Mater. Res. 42 (1998) 103–111.
[66] S.K. Schmiedberg, D.H. Chang, C.G. Frondoza, A.D.C. Valdevit, J.P. Kostuik, J. Biomed. Mater. Res. 28 (1994) 1277–1288.
[67] I. Catelas, D. Bobyn, J.B. Medley, J.J. Krygier, D.J. Zukor, A. Petit, O.L. Huk, J. Biomed. Mater. Res. 55 (2001) 320–329.
[68] H. Yue, W. Wei, Z. Yue, P. Lv, L. Wang, G. Ma, Z. Su, Eur. J. Pharm. Sci. 41 (2010) 650–657.
[69] U.E. Pazzaglia, C. DellOrbo, M.J. Wilkinson, Arch. Orthop. Trauma Surg. 106 (1985) 209–219.
[70] D.W. Murray, N. Rushton, J. Bone Joint Surg. 72 (1990) 988–992.
[71] J.J. Jacobs, A. Shanbhag, T.T. Glant, J. Black, J.O. Galante, J. Am. Acad. Orthop. Surg. 2 (1994) 212–220.
[72] N. Doshi, S. Mitragotri, PLoS ONE 5 (2010) e10051.
[73] A.S. Shanbhag, J.J. Jacobs, J. Black, J.O. Galante, T.T. Glant, J. Biomed. Mater. Res. 28 (1994) 81–90.
[74] P. Campbell, H. McKellop, R. Alim, J. Mirra, S. Nutt, L. Dorr, H.C. Amustutz, in: J.A. Disegi, R.L. Kennedy, R. Pillar (Eds.), Cobalt-base Alloys for Biomedical Applications, ASTM International, West Conshohocken, PA, 1999.
[75] K. Hashimoto, K. Asami, M. Naka, T. Masumoto, Corros. Sci. 19 (1979) 857–867.
[76] Y.H. Ma, B.C. Akis, M.E. Ayturk, F. Guazzone, E.E. Engwall, I.P. Mardilovich, Ind. Eng. Chem. Res. 43 (2004) 2936–2945.
[77] A. Pardo, M.C. Merino, A.E. Coy, F. Viejo, M. Carboneras, R. Arrabal, Acta Mater. 55 (2007) 2239–2251.
[78] I. Milogev, V. PiSot, P. Campbell, J. Orthop. Res. 23 (2005) 526–535.
[79] C.P. Case, V.G. Langkamer, C. James, M.R. Palmer, A.J. Kemp, P.F. Heap, L. Solomon, J. Bone Joint Surg. Br. 76 (1994) 701–712.
[80] R. Michel, M. Noite, M. Reich, F. Loer, Arch. Orthop. Trauma Surg. 110 (1991) 61–74.
[81] A.G. Cobb, T.P. Schmalzreid, Proc. Inst. Mech. Eng. H 220 (2006) 385–397.